Energy Reports 7 (2021) 3437–3448

Contents lists available at ScienceDirect

Energy Reports

journal homepage: www.elsevier.com/locate/egyr

Research paper

Energy saving of fans in air-cooled server via deep reinforcement learning algorithm

Wen-Xiao Chu, Yun-Hsuan Lien, Kuei-Ru Huang, Chi-Chuan Wang *

Department of Mechanical Engineering, National Chiao Tung University, 1001 University Road, Hsinchu 300, Taiwan

ARTICLE INFO

Article history:
Received 11 June 2020
Received in revised form 18 May 2021
Accepted 2 June 2021
Available online 11 June 2021

Keywords:
Deep reinforcement learning
Simulated server
Fan control
Energy saving

ABSTRACT

The present paper aims at using an artificial intelligence algorithm to minimize the fan power consumption in air-cooled servers. The proposed algorithm can handle the complex thermal environments within the servers to tailor the influences and interactions amid numerous heat sources, airflow, bypass phenomenon, fan operation, and the transient operations. Modified correlations are first proposed to effectively predict the thermal-hydraulic performance of heat sinks and the corresponding predictive ability against Nusselt number and pressure drop is within 5.0% and 10%, respectively. Without the algorithm control, the maximum deviation between the prediction and the experimental data is within 2.0 °C. By introducing the deep reinforcement learning (DRL) algorithm subject to the interactions of complex thermal environments, the fan power consumption can be saved by 55.7%, 40.3% and 26.3%, respectively, in comparison with the strategy with 100% fan duty. Yet the DRL agent still offers 16.7% energy saving when compared to a fixed 40% fan duty.

1. Introduction

With the advent of the information and communication technology (ICT) industry, the required capacity and loading regrading computing/transaction/processing/storage are exponentially increasing (Khattak and Ali, 2019). Yet servers play a kernel role to facilitate the gigantic demands within ICT systems, and the servers are usually grouped as clusters in data centers. The high-power chips are the main cores of the servers to carry out huge and diverse processing. Apart from their needs for high power consumptions, colossal heat is also generated. Consequently, it is imperative to apply effective thermal management strategy to limit the junction temperature below the threshold, which can maintain the high-efficient operational capability of servers. Some innovative cooling technologies were investigated for very high-flux electronics components, e.g., impingement cooling, water cooling and immersion cooling technologies. However, the air cooling strategy with heat sinks and fans is still the preferred method for featuring reliable and low-cost characteristics. Fig. 1 shows the internal layout of a typical 1U server (Chu et al., 2020) in which multiple heat sources are arranged, including two CPUs, RAMs, graphic card, network card, etc. Typical heat generation of each component ranges from 50 W to 250 W. The thermal environment can be improved by employing innovative fin configurations, such as VG (vortex generator) fins (Li et al., 2013; Yang et al., 2010), wavy fins (Lin et al., 2017), pin fins (Sara et al., 2001; Shaeri and Yaghoubi, 2009; Al-Damook et al., 2016; Maji et al., 2017) and non-uniform splayed fins (Kanyakam and Bureerat, 2011; Sparrow et al., 1980). In essence, the plate-fin structure is still the most widely used heat sink as far as the cost is concerned (Al-damook and Alkasmoul, 2018; Yu et al., 2005; Chen and Wang, 2017, 2018, 2016). On the other hand, fans are installed at the outlet to entrain airflow into the server to facilitate effective cooling. The fan duty may increase accordingly to respond the thermal loading to limit the junction temperature under the threshold requirement.

Usually, the fans are adjusted at several fixed revolutions which may also consume a certain amount of electric energy. Moreover, the higher fan revolutions are prone to acoustic noise. Hence, it is necessary to optimize the fan operation under an appropriate fan duty to save the power consumption and alleviate the noise level. Recently, the artificial intelligence (AI) control becomes more and more popular and is especially applicable for complex environments (Hua et al., 2019). The deep reinforcement learning (DRL) algorithm emerging from a powerful data-driven method can resolve complex problems in practical applications, which was successfully applied in playing Atari (Mnih et al., 2015) and Go games (Silver et al., 2016). Meanwhile, the DRL algorithm has been employed to control the HVAC (heating, ventilation and air-conditioning) system for improving energy efficiency (Dalamagkidis et al., 2007; Fazenda et al., 2014; Wei et al., 2017; Ma et al., 2012; Deodhar et al., 2015; Olivieri et al., 2014).

Fazenda et al. (2014) deployed the reinforcement learning algorithm to optimize the usage of HVAC system. A multi-objective

* Corresponding author.
E-mail address: ccwang@nctu.edu.tw (C.C. Wang).

https://doi.org/10.1016/j.egyr.2021.06.003

Nomenclature

A	Heat transfer area, m^2
a	Action
B	Width of heat sink, mm
c_1 and c_2	Coefficients
CB	Width of flow channel, mm
CH	Height of flow channel, mm
D_c	Hydraulic diameter, m
DRL	Deep reinforcement learning
f	Friction factor
Er	Calculating error
H_b	Height of heat sink base, mm
H_f	Fin height, mm
H_{tp}	Distance between thermocouples, m
H_{tot}	Total input heating load, W
h	Heat transfer coefficient, W m^{-2} K^{-1}
i	Row of heat source
L	Difference of Q
L_f	Length of fin region, mm
m_1 to m_5	Coefficients
Nu	Nusselt number
n_1 to n_5	Coefficients
P_f	Power consumption of fans
p	Pressure, Pa
Δp	Pressure loss, Pa
Q	Accumulated reward
q	Heat flux, W m^{-2}
Re	Reynolds number
r	Reward
s	State
T_{jun}	Junction temperature, K
t_f	Fin thickness, mm
t_p	Fin pitch, mm
Δt	Time step, s
v	Velocity, m s^{-1}
w	Weights

Greek symbols

γ	Decay factor
η	Learning rate
λ	Conduction coefficient, W m^{-1} K^{-1}
ρ	Density, kg m^{-3}
σ	Contraction ratio

Subscripts

bp	Bypass region
cd	Contraction and divergence section
exp	Experimental data
f	Fin region
fr	Friction
l	Laminar
in	Inlet
pre	Predicted result
t	Turbulent

optimal supervisory control containing the activity schedules, occupancy patterns, individual thermal comfort preferences of each occupant and the cost of energy should be considered. Dalamagkidis et al. (2007) developed a linear reinforcement learning controller to improve the thermal comfort of building occupants and indoor air quality with lower energy consumption. Wei et al. (2017) validated that the DRL algorithm can achieve up to 20%–70% energy cost reduction compared to traditional algorithm approaches. Ma et al. (2012) developed a nonlinear model for controlling the overall HVAC system, including chillers, cooling towers and thermal storage banks. The improvement on COP (coefficient of performance) may reach 19.1% averagely, and the better COP can be achieved with average ambient temperature ranging between 12–18 °C compared to the original control logic. Deodhar et al. (2015) presented a coordinated, real-time monitoring and control algorithm that could evaluate the thermal health of the data center through its intelligent temperature analyzer. As the result, a systematic increase in the set points of the cooling units from 24 °C to as high as 28 °C was observed, resulting in an overall energy-saving of 9% in the cooling demand. Lucchese and Johansson (2019) tried to manage the thermal state of data servers by provisioning their cooling airflow dynamically. A thermal network framework was introduced which can capture the temperature dynamics of the on-board thermal inertia.

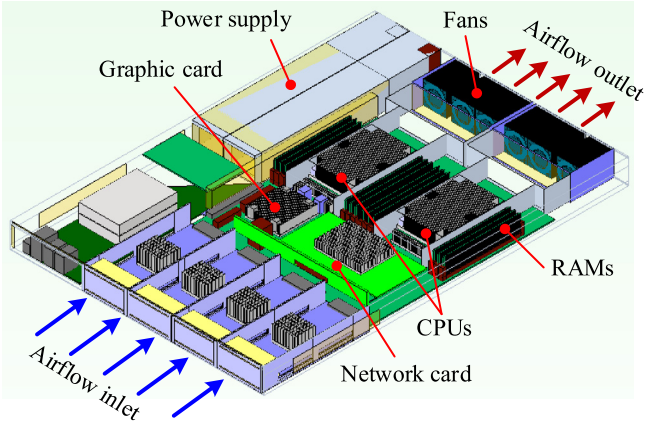

Fig. 1. Schematic of typical layout in a 1U server (Chu et al., 2020).

The reinforcement learning algorithm was also successfully implemented as an optimized control strategy for energy management. Kuznetsova et al. (2013) adopted the reinforcement learning algorithm for the energy management with the optimal actions for battery scheduling under different time-dependent environmental conditions. Zhang et al. (2018) introduced the DRL algorithm to control the supply water temperature of the radiant heating system of an office building. It was tested that the best trained DRL strategy can save up to 15% of heating energy with similar indoor thermal comfort compared to the base case. Kazmi et al. (2018) presented a novel reinforcement learning based methodology to optimize energy consumption for hot water production systems in Netherlands. The annual energy consumption could be roughly saved by 200 kWh for a single household without the loss of occupant comfort. Xi et al. (2018) also proposed a novel strategy based on reinforcement learning algorithm to solve the stochastic disturbance caused by the massive integration of the renewable energy and compatibility associated with original power system. Compared to other smart methods, their proposed algorithm converges faster and contains stronger robustness to reduce carbon emission and enhance utilization rate of the new energy. Zhang et al. (2019) proposed a novel memetic reinforcement learning algorithm for harvesting the maximum available solar power under different weather conditions in photovoltaic (PV) systems. Comprehensive cases were studied and

results showed that the PV system is enabled to generate higher energy with smallest power fluctuations when compared to other traditional meta-heuristic algorithms in different seasons. Cheng et al. (2016) developed an improved Q-learning controller, which can provide an improved indoor luminous environment. The algorithm showed a high user acceptance with better thermal comfort and an attainable energy-saving up to 10%. Claessens et al. (2018) introduced the reinforcement learning strategy to optimize the thermostatically controlled loads connected in a district heating network. A significant performance improvement was achieved after a learning period of 40–60 days.

As one of the most popular intelligent control strategies, the DRL has been widely applied for microgrid optimization, speech recognition, language translation, robotic technology, industrial automation, etc., which can dramatically improve the system performance and corresponding efficiency. The most important characteristics of DRL algorithm is that the deep neural networks can automatically find the optimal results or features in high-dimensional data sets. It has similar benefits in comparison to reinforcement learning (RL). However, the DRL algorithm has accelerated objective detection capability. Thus, the DRL algorithm is involved to control the server fans, aiming to achieving considerable energy savings with the background of global carbon neutrality. Valladares et al. (2019) proposed a DRL algorithm to resolve complex interactions between thermal comfort, energy consumption and indoor air quality. The preceding studies adopted AI to tailor the environments in connection with human comfort and energy saving. Regarding the main cores of the AI systems — servers in data center, very rare studies were made available through AI based methods upon the energy-saving potential. Note that the power consumption of the cooling systems is normally comparative to IT equipment (Ni and Bai, 2017). Yet the thermal management inside the server rack is quite complicated due to multi-heat sources with varying power, various heat sinks profiles, and variable air flowrate with appreciable bypass airstream that does not enter the heat sink. In this regard, it is the purpose of this study to introduce an AI based algorithm to manage the complex thermal environment with maximum energy-saving potential. The present study proposes a DRL algorithm to optimize to fan control strategy in a simulated server to minimize fan energy consumption without overheating the electronics devices.

2. Experimental system

2.1. General description

For achieving the data sets of heat transfer performance of multiple heat sources, the experimental system is established. Fig. 2 depicts the schematic of experimental system of the simulated server, which contains heat sources, heat sinks and fans. Two power supply units and power meters are used to provide and to measure the input heat loading from the heat sources and the fan power. The cold air is induced to the server cabinet by the fan array. The operating parameters such as the junction temperature of heat sources, air inlet/outlet temperatures and fan duty are recorded by the Raspberry Pi, which is able to interpret and build control strategy based on DRL algorithm, and finally the command logic is directed to fan duty control.

Fig. 3 illustrates the configuration of heat source units. A heater which can generate a maximum power of 150 W is placed at the bottom, and a copper plate is adhered on the heat source with silicon grease for reducing the thermal contact resistance. A T-type thermocouple is embedded at the center to measure the temperature of cooper plate, which is regarded as the junction temperature of the heat source. The heat sources can move horizontally alongside the acrylic board to simulate the influence of

Table 1
Distribution of thermal resistance.

Thermal resistance	Location	Material	R /K W^{-1}
R_{air}	Airflow	–	–
R_{hs}	Fin	Aluminum	$3.5\times10^{-2}\sim 4.88\times10^{-2}$
R_{TIM}	TIM	Silicon grease	$1.0\times10^{-3}\sim 2.0\times10^{-3}$
R_{ht}	Heater	Ceramic	0.02∼0.0347
R_{ac}	Supporting layer	Acrylic	20–25
R_{w}	Insulation layer	Wood	70–75

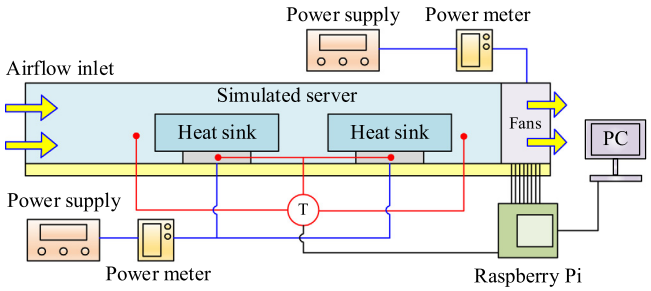

Fig. 2. Schematic of experimental system.

locations with different heat source layouts. For reducing the heat loss from the server shell, an insulated wood board is installed beneath the acrylic board as the base surface. The thermal resistance distribution is shown in Table 1. Note that the thermal resistance below the heat source is 3–5 orders higher than that beyond the heat source. Hence, the major heat will dissipate from heat sinks and is carried out by convective airflow.

The configurations with single-heat source and multi-heat sources are respectively tested, which are shown in Fig. 4(a) and (b). The geometrical parameters of the simulated server are 480 mm (width) × 600 mm (depth) × 44 mm (height), whose dimension is similar to the 1U server. The dimensions of fans are 40 mm × 40 mm × 28 mm. The rectifier net with the porosity of 60% is installed at the upstream to simulate the flow resistance of the perforated plate in actual servers. The inlet/outlet temperatures are measured by thermocouple arrays. The velocity of induced airflow is measured by hot-wire anemometers after the airflow passing the inlet rectifier net. The insulation wools with the conductivity of 0.2 W m^{-1} K^{-1} are placed at the side and top to prevent heat loss through outer surfaces. The corresponding fan curve is shown in Fig. 5. The maximum volumetric flowrate of a single fan can reach 21.5 CFM (corresponding to a fan duty of 100%) without pressure resistance.

2.2. Data reduction

Fig. 6(a) and (b) shows the front view and top view of a single heat sink. Two configurations are applied with the same base height, fin thickness and fin pitch, and Table 2 tabulates the corresponding geometrical parameters. Note that part of the airflow may enter fin channels of the heat sink to facilitate effective heat dissipation, and the other part may bypass the heat sink without heat removal. Note that the bypass airflow may impose remarkable influence on the performance of heat sink (Prstic and Bar-Cohen, 2006; Li et al., 2012, 2010). By considering the influence of fan curve, the airflow velocity in fin region (v_f) may

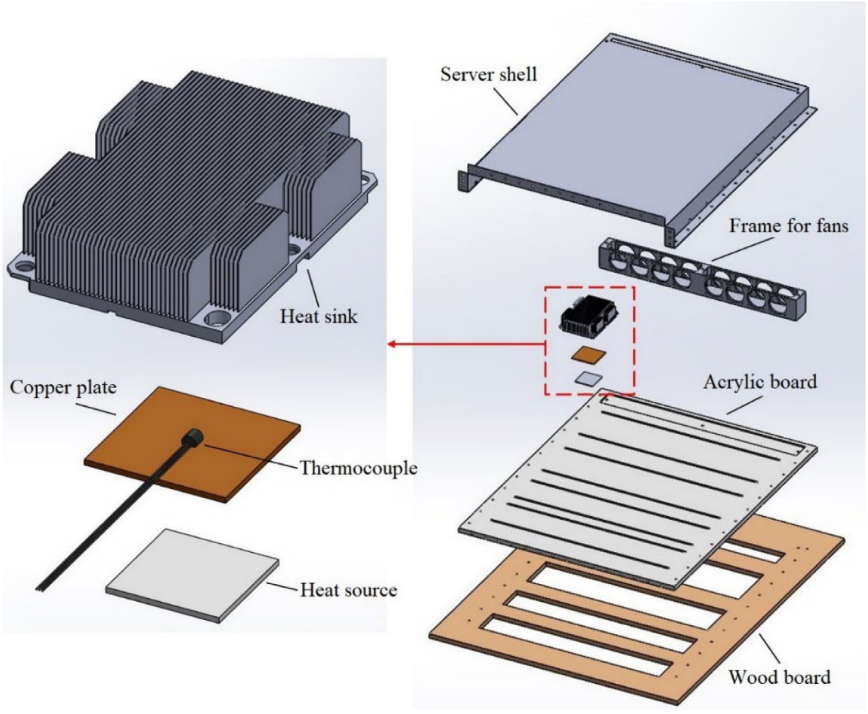

Fig. 3. Configuration of heat source.

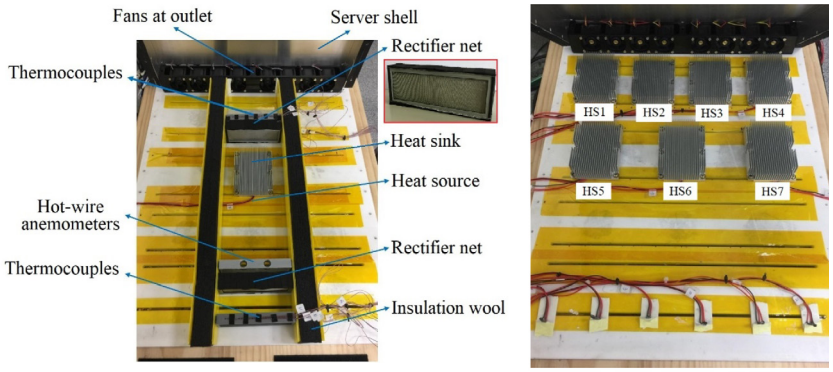

(a) test for single heat sink (b) test for multiple heat sinks

Fig. 4. Layout for testing single/multiple heat sources.

closely interrelate to the pressure drop along flow direction (Δp_i). The actual v_f and Δp_i can be calculated via indirect method in the following. The Bernoulli equation is applicable along the flow direction, which can be expressed as follows:

$$p_i + \frac{1}{2}\rho v_{in}^2 = p_{i+1} + \frac{1}{2}\rho v_f^2 + \Delta p_{cd,f} + \Delta p_{fr,f} \quad (1)$$

$$p_i + \frac{1}{2}\rho v_{in}^2 = p_{i+1} + \frac{1}{2}\rho v_{bp}^2 + \Delta p_{cd,bp} + \Delta p_{fr,bp} \quad (2)$$

where p_i and p_{i+1} are the static pressures at the inlet and outlet of heat sinks in the i row, v_{in} is the average velocity at the inlet, v_f and v_{bp} are the local average velocity entering fin region and bypass region, respectively, $\Delta p_{cd,f}$ and $\Delta p_{cd,bp}$ represent the pressure drop at contraction and expansion sections while $\Delta p_{fr,f}$ and $\Delta p_{fr,f}$ are the corresponding friction pressure drop which is related to the Fanning friction factor (f) by Eqs. (3) and (4).

$$\Delta p_{fr,f} = f\frac{L_f}{D_c}\cdot\frac{1}{2}\rho v_f^2 \quad (3)$$

Table 2
Geometrical parameters of heat sinks.

Variables	Parameters (mm)
Heat sink length and width ($L_f \times B$)	Type A: 108 × 78 Type B: 80 × 80
Fin height (H_f)	21
Fin pitch (t_p)	2.6
Fin thickness (t_f)	0.7
Base height (H_B)	4.2

$$\Delta p_{fr,bp} = f\frac{L_f}{D_c}\cdot\frac{1}{2}\rho v_{bp}^2 \quad (4)$$

The friction factor for turbulence and laminar regimes can be calculated by Eqs. (5) and (6), respectively.

$$f_t = \frac{0.3164}{Re^{0.25}} \quad (5)$$

$$f_l = \frac{64}{Re} \quad (6)$$

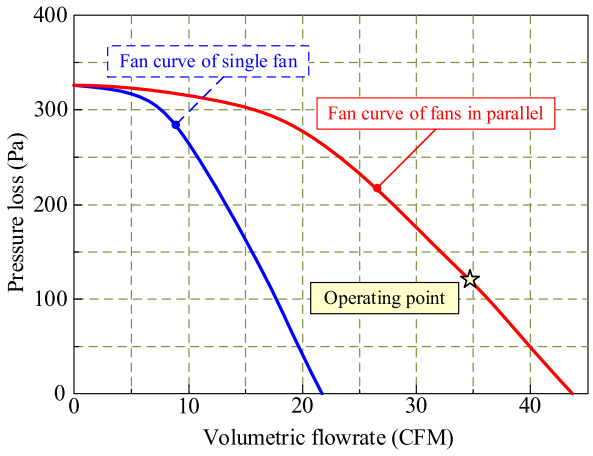

Fig. 5. Fan curve characteristics.

Table 3
Hydraulic parameters for fin region and bypass region.

Variables	Fin region	Bypass region
Velocity definition, v	v_f	v_{bp}
Hydraulic diameter, D_c	$D_{c,f} = \frac{4H_f \times t_p}{2(H_f + t_p)}$	$D_{c,bp} = \frac{4A_{bp}}{2(CB + CH + H_f)}$
Reynolds number, Re	$Re_f = \frac{\rho v_f D_{c,f}}{\mu}$	$Re_{bp} = \frac{\rho v_{bp} D_{c,bp}}{\mu}$
Area ratio, σ	$\sigma_f = \frac{B}{(N-1)t_p}$	$\sigma_{bp} = \frac{CB \times CH}{CB \times CH - B \times H_f}$

The $\Delta p_{cd,f}$ and $\Delta p_{cd,bp}$ shown in Eqs. (1) and (2) can be estimated regarding the contraction ratio (σ) (Jonsson and Moshfegh, 2001):

$$\Delta p_{cd} = \left(1.3947 - 1.9611\sigma - 1.4026\sigma^2\right)\frac{1}{2}\rho v_{in}^2 \tag{7}$$

Table 3 illustrates the definition of hydraulic parameters using for the fin region and bypass region, respectively. In essence, the heat sink structure and bypass region is critical to the pressure loss across a single heat sink (Δp_i), and an empirical correlation was developed by (Jonsson and Moshfegh, 2001):

$$p_{i+1} - p_i = \Delta p_i = c_2 \left(\frac{Re}{1000}\right)^{n_1} \left(\frac{CB}{H_f}\right)^{n_2} \left(\frac{CH}{H_f}\right)^{n_3} \times \left(\frac{t_f}{H_f}\right)^{n_4} \left(\frac{t_p}{H_f}\right)^{n_5} \tag{8}$$

where CB is the flow channel, CH is the height of flow channel, H_f is the height of heat sink, t_f and t_p are the fin width and fin pitch, respectively. Then, the pressure drop from server inlet to server outlet is obtained by Eq. (9).

$$\Delta p_{tot} = \sum_{i=1}^{N} (p_{i+1} - p_i) = \sum_{i=1}^{N} \Delta p_i \tag{9}$$

As aforementioned, Δp_{tot} may also affect the volumetric flowrate due to the impact of fan curve. The operating point of the fan array at fixed fan duty can be identified via iteration. Similarly, the Nusselt number of specific heat sink can be calculated by Eq. (10), which was also validated by (Jonsson and Moshfegh, 2001).

$$Nu = c_1 \left(\frac{Re}{1000}\right)^{m_1} \left(\frac{CB}{H_f}\right)^{m_2} \left(\frac{CH}{H_f}\right)^{m_3} \left(\frac{t_f}{H_f}\right)^{m_4} \left(\frac{t_p}{H_f}\right)^{m_5} \tag{10}$$

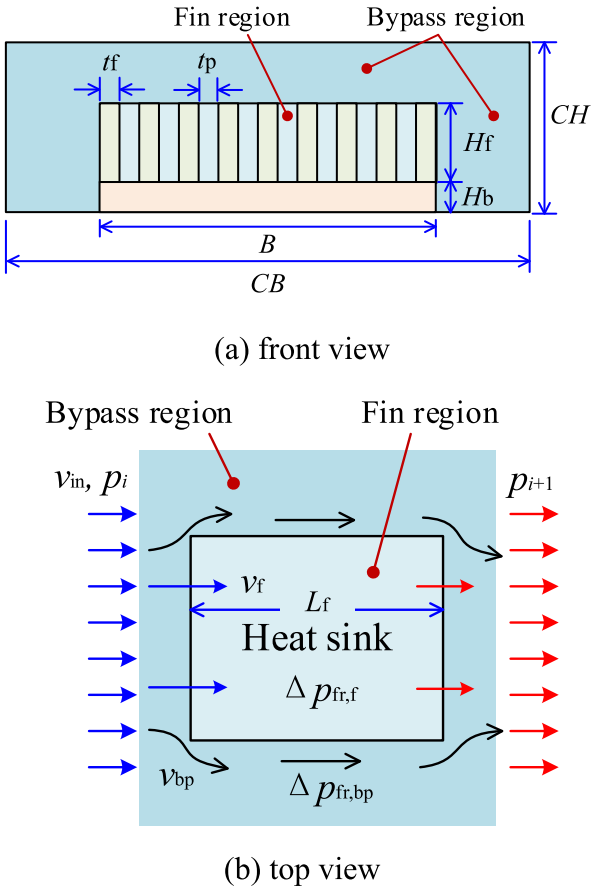

Fig. 6. Schematic of geometrical parameters and airflow distribution.

Fig. 7 shows the schematic of airflow distribution in the simulated server installing with multiple rows of heat sinks having staggered layout. Note that some of the cold airflow may directly bypass the front heat sinks to be in contact with next row heat sinks with a much higher temperature difference. It is assumed that the airflow in the front fin region may well mix with adjacent bypass airflow in the overlapped zone before entering the next fin region. The average inlet temperature is applied for each heat sink. For electronic cooling, maintaining the junction temperature (T_{jun}) below the threshold is the major concern regarding long-term reliability (Klitzke et al., 2018). The T_{jun} can be calculated by Eq. (11) and the predictive deviation can be calculated by Eq. (12).

$$T_j = T_{in} + \frac{q}{hA} = T_{in} + \frac{q}{\frac{Nu \cdot \lambda}{D_{c,f}} A} \tag{11}$$

$$Er = \frac{T_{jun,pre} - T_{jun,exp}}{T_{jun,exp} - T_{in}} \tag{12}$$

3. Algorithm description

3.1. DRL algorithm procedures

The DRL algorithm is a powerful data-driven method, which can achieve the cognition to a specific environment after the continuous update of data set (Mnih et al., 2015). Figs. 8 and 9 illustrate the architecture diagram and flowchart of the present main DRL algorithm for server performance evaluation and fan control, including a data sample loop, control loop and learning loop. The utilization of the DRL algorithm based on the Markov decision process was proved to be a viable solution for energy

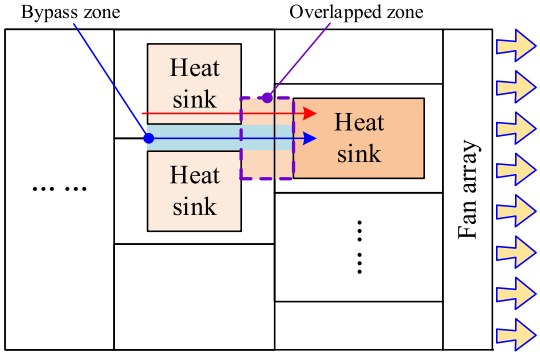

Fig. 7. Schematic of airflow distribution in the server.

saving in the HVAC system (Dalamagkidis et al., 2007; Wei et al., 2017; Zhang et al., 2018; Valladares et al., 2019). The DRL agent along with the ANN is applied, which has combines artificial neural networks with a reinforcement learning architecture. The agent can successfully stabilize the action control. As the result, the algorithm is capable to learn the best actions in order to attain the energy-saving without overheating the electronics devices.

The establishment of data sample sets aims to explore the change of thermal state after taking random actions. The system states include the fan duty, volumetric flowrate, junction temperature (T_{jun}) of heat sources and some intermediate parameters like Δp_{tot}, v_f and Re. The control of fan duty is regarded as actions. Once the action is executed, the record of resulting experience on changed states as well as the reward would be saved into the memory which contains the original state (s_{t-1}), action (a_t), resultant state after the action execution (s_t) and the reward (r_t). This cycle may repeat indefinitely over time until the memory set contains enough experience to train the neural networks. Then, the data sample loop ends and the control loop and learning loop start.

Basically, the random actions in the initial memory perform exploration process. It is indicated that the exploration phase will transfer to the exploitation phase with the help of learning loop. Mini-batch of experience may import to the neural network algorithms. The learning process allows the algorithm to study from the past experience and the weights may keep updated in the neural network, aiming to suggest a better decision. The error back-propagation (BP) method is implemented. It should be stressed that the only function of the target network ($\hat{Q}$) is to train the main network (Q) with the objective of minimizing the gradient of loss between the Q-network and Q̂-network. The weights in the Q-network are continuously updated to give better predictions. Meanwhile, the Q-network may share its learned

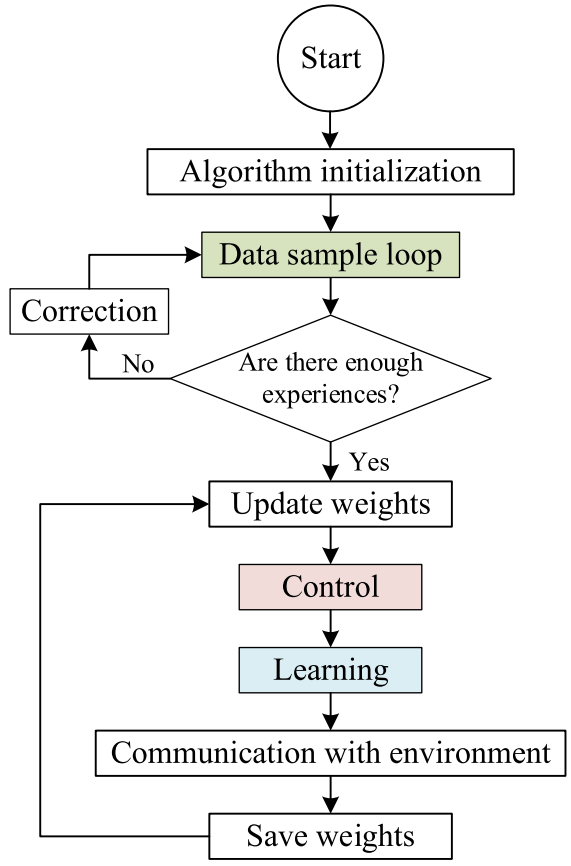

Fig. 9. Flowchart of DRL algorithm.

information to the Q̂-network at the end of the learning process by a soft update on weights.

With the accumulated experience and knowledge growth during the learning process, the action yielding the maximum reward will be exploited. As the result, the DRL algorithm can get the maximum reward and correctly output the optimal action which will be executed in the control process.

3.2. Reward criteria

In the experimental system, the initial T_{jun} of heat sources is measured by thermocouples. Then, the actions are adopted, regardless good or bad, which can be evaluated via the reward function, r. Note that the goal of minimizing fan power consumption contradicts the goal of maintaining the T_{jun} of heat sources

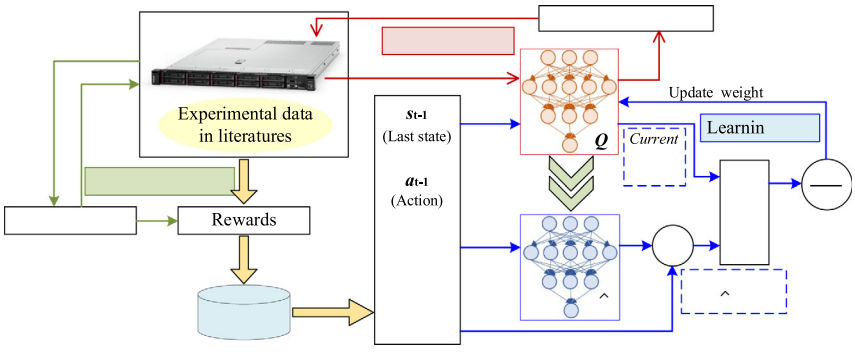

Fig. 8. Architecture diagram of DRL algorithm.

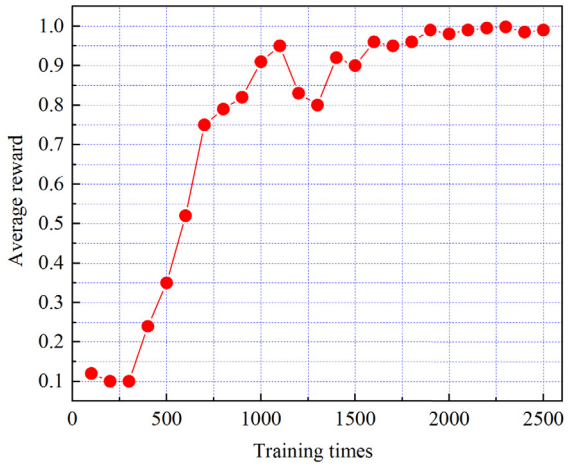

Fig. 10. Variation of average reward with increasing training times.

to be as low as possible. The reward function for actions without over-temperature conditions is defined as follows:

$$r = 0.9\left[\frac{\text{atan}\left(H_{tot}/P_f\right) - 15}{\pi} + 0.5\pi\right] + 0.1 \tag{13}$$

where H_{tot} is the total input heating load, P_{f} is the power consumption of fans. The arc-tangent function is used with the consideration for limiting the reward value in a certain range, which can improve the convergence during the training process. This is because the value of temperature and energy consumption may not vary significantly. The reward is defined as the value close to 0.1 when the optimal action is executed.

The present study also updates the Q value estimation by the Q-learning method with implicit strategy, which is shown as follows (Watkins and Dayan, 1992):

$$Q\left(s_{t+1}, a_{t+1}\right) = Q\left(s_t, a_t\right) + \eta\left[r_{t+1} + \gamma \max_{a_{t+1}} Q_t\left(s_{t+1}, a_{t+1}\right) - Q\left(s_t, a_t\right)\right] \tag{14}$$

where a_{t} and $a_{\text{t+1}}$ represent the last control action and the deterministic next control action, s_{t} and $s_{\text{t+1}}$ are the predicted states after the action a_{t} and $a_{\text{t+1}}$, η represents the learning rate during learning process, γ is the decay factor of the maximum reward. As the result, the maximum accumulative reward can be obtained after taking optimal actions over time. Fig. 10 illustrates the average reward in variation of training times. Note that very low average rewards are received when the training time is less than 400 because inexperienced random actions are executed. Then, the average reward is growing rapidly when training times rising to 1000, indicating that the agent becomes more experienced and proficient. Afterwards, the average reward may temporarily fluctuate during the period of experience accumulation and reach close to 1.0 after increasing the training time to 1800.

4. Results and discussion

4.1. Validation of correlations

As aforementioned, the heat sink configuration, bypass space and the Reynolds number plays essential role on thermal management. The correlation coefficients to describe the pressure drop and heat transfer as depicted in Eqs. (8) and (10) are shown in Table 4 (Jonsson and Moshfegh, 2001). The correlations are applied to verify the experimental data from Hossain (2006), Butterbaugh and Kang (1995), Yuan (1996), Lee (1995) and Li et al. (2009), respectively. The comparison is illustrated in Fig. 11(a). It is found that the Nusselt number is always overestimated and the pressure drop is underestimated. This is mainly because the height of heat sink base (H_{b}) is not considered. Meanwhile, a wide range of geometric parameters of heat sinks is involved subject to broader application.

Table 4
Correlation coefficients for Nusselt number in literature.

	c_1	n_1	n_2	n_3	n_4	n_5
Nu	4.783	−0.4778	−0.6874	−0.5979	−0.7184	0.6736
	c_2	m_1	m_2	m_3	m_4	m_5
Δp	88.28	0.6029	−0.1098	−0.5632	0.08713	0.4139

In this regard, the correlations have to focus on specific plate-fin heat sinks. Experimental results on single heat source and multiple heat sources are also employed for higher prediction accuracy. Meanwhile, the airflow would also be blocked by the heat sink base, resulting in significant variation on airflow distribution. Meanwhile, the heat sink base may also pronouncedly affect the fin efficiency. Hence, the H_{b} should be considered by introducing the parameter of $(CH - H_{\text{b}})/H_{\text{f}}$, and the new correlations are shows as follows:

$$\Delta p_i^* = 4.703\left(\frac{Re}{1000}\right)^{-0.5974}\left(\frac{CB}{H_f}\right)^{-0.2547}\left(\frac{CH - H_b}{H_f}\right)^{-0.7111} \times \left(\frac{t_f}{H_f}\right)^{-0.8087}\left(\frac{t_p}{H_f}\right)^{0.4772} \tag{15}$$

$$Nu = 88.28\left(\frac{Re}{1000}\right)^{0.5308}\left(\frac{CB}{H_f}\right)^{-0.4239}\left(\frac{CH - H_b}{H_f}\right)^{-0.7761} \times \left(\frac{t_f}{H_f}\right)^{0.09408}\left(\frac{t_p}{H_f}\right)^{0.4321} \tag{16}$$

Through this modification of Eqs. (8) and (10), the predictive abilities against the experimental data from Hossain (2006), Butterbaugh and Kang (1995), Yuan (1996), Lee (1995) and Li et al. (2009) are significantly improved as shown in Fig. 11(b). Note that the Nu and Δp are estimated within 20% and 30%, respectively. Yet the prediction of Nu and Δp on experimental data in present study can be controlled by up to 5.0% and 10%, respectively. This is mainly because that the bypass flow which do not contribute to heat transfer with heat sinks is considered as corrections in the empirical correlations.

On the other hand, the time step in DRL algorithm may significantly affect the predictive accuracy and computational load.

Fig. 12 illustrates the effect of time step on the prediction of T_{jun}. Note that the estimated error shows exponential increase with the rise of computational time step. It can be found that the maximum error of T_{jun} with the time step of 0.1 s, 0.5 s and 1.0 s may reach 17.0%, 18.5% and 21.8%, respectively. Meanwhile, the computation load for the case with $\Delta t = 0.1$ s is about five times greater when compared to the case with $\Delta t = 0.5$ s. Hence, the computing time step with 0.5 s is regarded as a more economic strategy.

4.2. Performance prediction

During the transient operation of servers, the current operating states after taking actions should be accurately predicted. In our prior study, the T_{jun} of heat sources is applied as the most crucial criterion for evaluating the thermal performance of

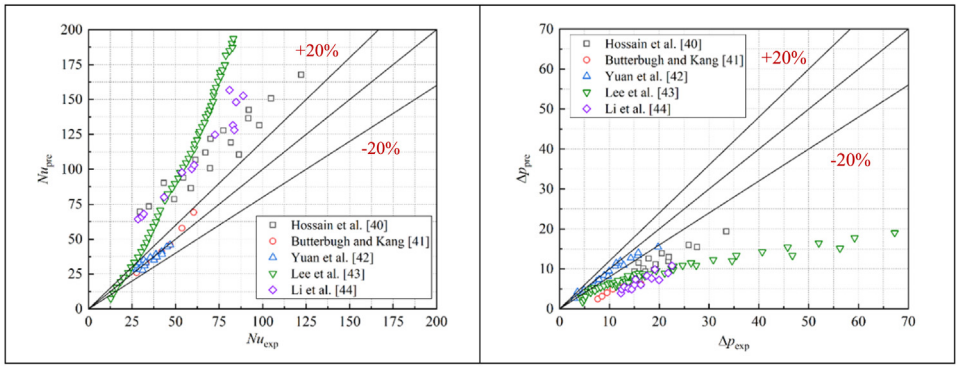

(a) predictions of Nu and Δp in literatures

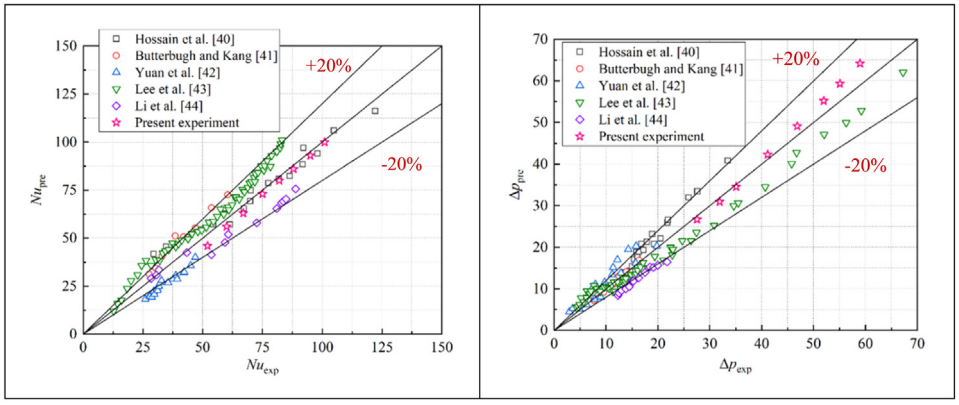

(b) predictions of Nu and Δp in present paper

Fig. 11. Prediction accuracy of correlations with proposed coefficients in the literatures and that in present paper.

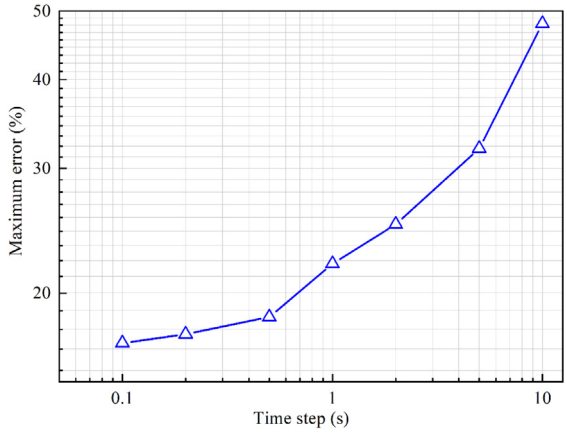

Fig. 12. Maximum error of Tjun in variation of time step.

heat sinks, which can be predicted by Eq. (11) from the thermal resistance analysis. Fig. 4(b) shows the T_{jun} for seven heat sources with two-row layout. The initial heating load of seven heat sources and the fan duty of eight fans are 53 W and 100%, respectively. The T_{jun} is recorded as $t = 0$ s after the system reaching steady state. Table 5 demonstrates the key parameters in the applied DRL algorithm. Notice that the over-temperature phenomena may happen after decreasing fan duty and rising heating load, indicating possible failure of the system. In this regard, the prediction accuracy during above processes must be examined.

Table 5
Parameter setting for DRL.

Actor learning rate	0.00001
Memory capacity	2300
Mini-batch size	1000
Learning rate	0.0001
Decay factor	0.7
Soft update factor	0.001
Neural network size	5 layers and 100 nodes
Activation function	ReLU

Fig. 13(a) shows the variation of T_{jun} when reducing the fan duty from 100% to 50%. The heating load of heat sources remains unchanged. Notice that the first-row heat sources usually contain lower temperatures for facing the low airflow temperature of the incoming airflow. Alongside the flow direction, the heat transfer at the rear part of servers may suffer from higher airflow temperatures. Since the heat sources are arranged with nearly symmetrical layout, the temperature distribution also shows almost symmetrical manners. Due to the non-uniform airflow distribution, the T_{jun} of center heat sources at the second row (HS2 and HS3) is lower than those heat sources located at the edges (HS1 and HS4). This can be explained from the layout configuration shown in Fig. 4(b). Part of airflow may bypass the heat sink of HS6 and directly enter the fin region of HS2 and HS3, yielding better heat transfer performance accordingly.

Fig. 13(b) depicts the variation of T_{jun} while raising the heating load of six heat sources (HS1, HS2, HS3, HS4, HS5 and HS6) to 78 W, and one heat source (HS7) to 100 W. The predictions and experimental measurements, as seen in the figure, are in good agreement. The predictive deviation can be calculated via

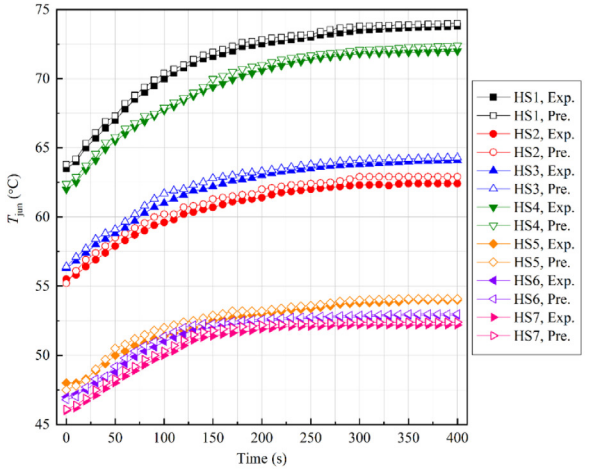

(a) fan duty decreasing process

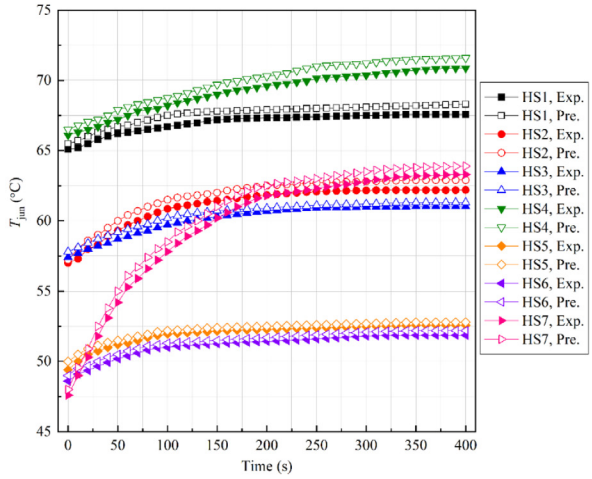

(b) heat load rising process

Fig. 13. Prediction of T_{jun} in the server with multiple heat sources.

effective temperature difference, e.g. Eq. (12). The maximum temperature deviations is about 2.0 °C, and the maximum deviation is 10.4% which occurs at the beginning of abrupt adjustments of increasing heating load increasing and reducing fan duty. The average prediction deviation is 6.2% and the predicted T_{jun} is always overestimated which can ensure the safety operation of apparatus. In essence, the proposed DRL algorithm combining with proposed correlations not only shows reasonable prediction on T_{jun}, but also ensures safe operation during transient periods.

4.3. AI control with DRL algorithm

The implemented heat sinks are in two specifications and the dimensions are shown in Table 2. Initially, the heating load of all heat sources remains at 100 W and the fans are adjusted to fix the T_{jun} of HS4 at 80 °C. Subsequently, the DRL control strategy is triggered to compare the strategies having fixed fan duties of 100%, 80%, 60% and 40%, respectively. The training of DRL algorithm is initiated in specific ranges tabulated in Table 6. In an actual server, the heat source number and layout, heating load and fan number may change from case to case. Based on preceding analysis, the heat sources at the edges are comparatively critical to overheating. Hence, the T_{jun} of HS4 is recorded for

Table 6
Applicable ranges.

Variables	Applicable range
Heating load	70 to 150 W
Threshold of junction temperature	105 °C
Heat sink rows	2 to 4
Fan number	6 and 8

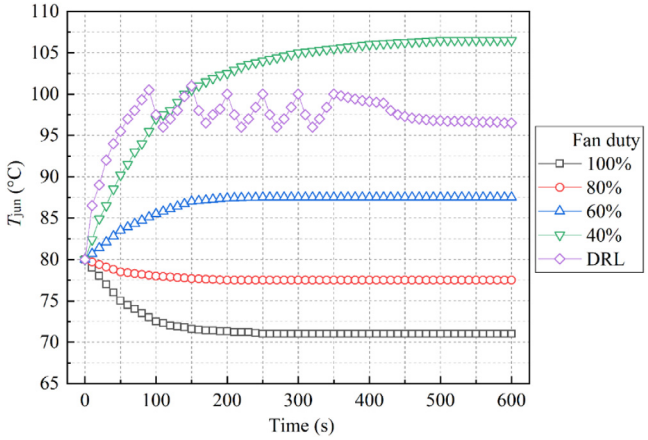

Fig. 14. Variation of T_{jun} in case 1.

comparison. A total of four cases are tested and the configurations are described in Table 7.

Case 1 installs with ten heat sources in three rows. The heat sinks with the size of 108 mm × 78 mm × 21 mm are arranged for heat sources HS1 to HS6, and the size 80 mm × 80 mm × 20 mm are installed for heat sources HS7 to HS13. Eight fans are implemented. The measurements start when triggering the heating load of HS1 to HS4 from 100 W to 150 W. As shown in Fig. 14, The T_{jun} gradually raises and reaches over 106 °C at a fixed fan duty of 40%. The operation with the fan duty of 60% can maintain the T_{jun} at 87.5 °C after 200 s, which is lower than the threshold setting point (100 °C). When fan duty reducing to 40%, the T_{jun} may exceed the setting point. On the other hand, the T_{jun} fluctuated when the fans are controlled by DRL algorithm. This is because the lack of experience at the beginning where the algorithm control cannot make the optimal decision to minimize the fan duty initially. After the running 350 s, the DRL adapt to adjust itself and the fluctuation of T_{jun} is eliminated to yield a stable fan operation.

For case 2, the configuration is the same with case 1. First, the heating load of heat sources HS1 to HS4 also rises from 100 W to 150 W. As shown in Fig. 15, the fluctuation period of T_{jun} by DRL algorithm is shortened to 200 s, meaning the control algorithm becomes more experienced and gains better predictive ability. Then, the heating load reduces to 70 W after the operation time reaching 300 s. The T_{jun} gradually decreases and the fluctuation of T_{jun} disappears. Compared to the case of fixed fan duty of 40%, the T_{jun} is well controlled by DRL algorithm and maintain at a higher level with lower fan duty to save fan power. In summary, the fan power consumption is effectively reduced by the DRL control agent.

Case 3 introduces three more heat sources (HS11, HS12 and HS13) at the position near the airflow inlet, which also operate at 100 W. Then, the heating load of HS1 to HS4 changes from 100 W to 150 W. Fig. 16 shows the variation of T_{jun}. Note that the fluctuation still exists when facing an inexperienced case. The T_{jun} becomes higher when compared to case 2 due to more severe thermal environment of HS4. Eventually, the T_{jun} is controlled around 97.5 °C by implementing the DRL algorithm control.

Table 7
Description of four cases.

	Heat source/fan number and layout	Change of heat loading (HS1 to HS4)	Fan number
Case 1	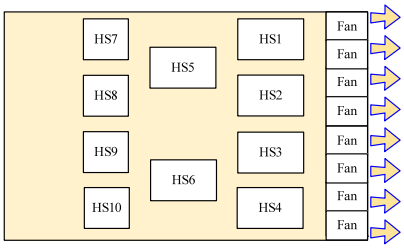	100 W to 150 W	8
Case 2		100 W to 150 W to 70 W	8
Case 3	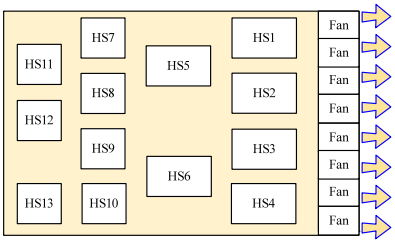	100 W to 150 W	8
Case 4	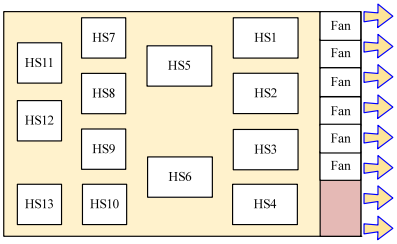	100 W to 150 W	6

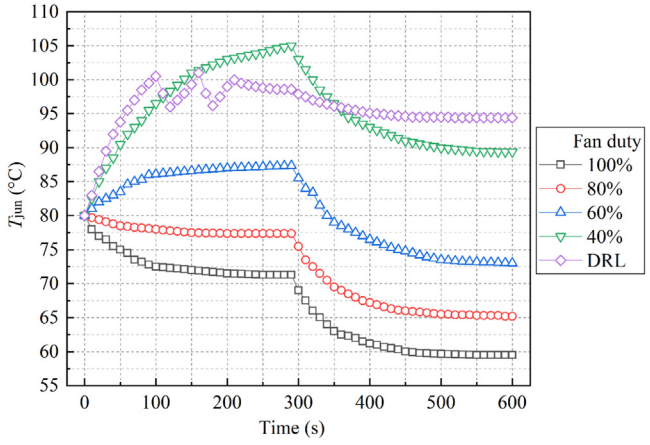

Fig. 15. Variation of T_{jun} in case 2.

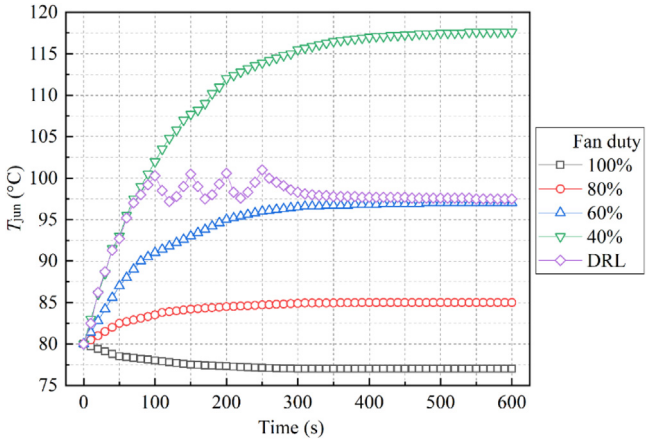

Fig. 16. Variation of T_{jun} in case 3.

For case 4, the same heat source layout and heating load distribution with case 3 are implemented. However, the fan number decreases from eight to six, indicating a more severe operating condition. As described in Fig. 17, the T_{jun} with the fan duty of 60% may reach 110 °C. Meanwhile, the fluctuation controlled by algorithm is obviously alleviated, indicating that the control strategy makes better decision than that in prior cases. Meanwhile, the T_{jun} is more close to the threshold setting point of junction temperature, suggesting a more precise control.

Fig. 18 shows the power consumption of four cases subject to various control strategies. For the cases of increasing heating load (cases 1, 3 and 4), the DRL control strategy can save the power consumption of fans by 55.7%, 40.3% and 26.3%, respectively, in comparison with the strategy with 100% fan duty. As the heating load decreasing shown in case 2, the power consumption of fans is still saved by 16.7% when compared to the strategy with a fixed 40% fan duty. In summary of the foregoing discussion, it

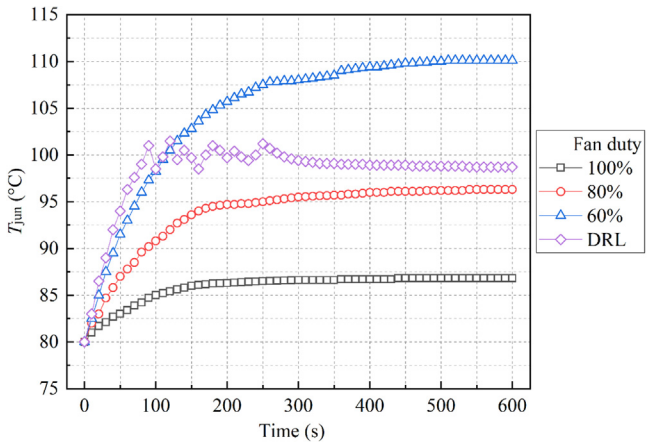

Fig. 17. Variation of Tjun in case 4.

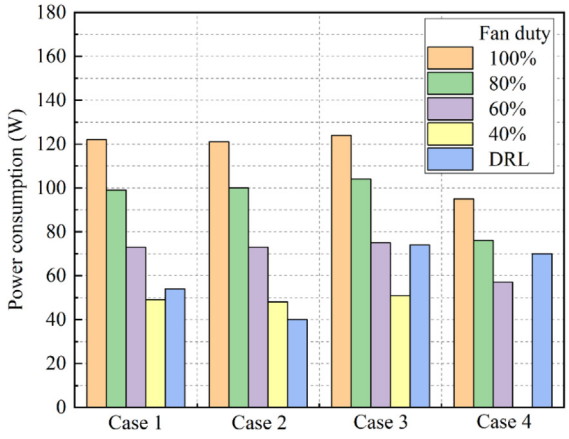

Fig. 18. Comparison of power consumptions.

is concluded that the proposed DRL algorithm is capable to save substantial energy when applying in a large-scale data center.

5. Conclusions

The present paper study adopts an artificial intelligence algorithm to minimize the fan power consumption in air-cooled servers. The proposed algorithm can handle the complex thermal environments within the servers to tailor the influences and interactions amid numerous heat sources, airflow, bypass phenomenon, fan operation, and the transient operations. Modified correlations are developed to describe the thermal-hydraulic performance of heat sinks. The correlations can well predict the Nusselt number and pressure drop of the plate heat sink. Then, the DRL algorithm, including a data sample loop, control loop and learning loop, is adopted to curb the complex thermal environment in a simulated server with multiple heat sources. Based on the foregoing discussions, the following conclusions are drawn:

(1) The developed empirical correlations can well predict the existing experimental data of heat sinks having plate fin configurations. The predictive ability in terms of Nusselt number and pressure drop against experimental results are within 5.0% and 10.0%, respectively.
(2) Through the training by the proposed DRL algorithm associated with the developed thermo-fluid correlations for plate heat sinks, the transient variations of the junction temperature for multi heat sources can be well predicted. The predicted junction temperature is always slightly overestimated to ensure the safety operation of server system. The maximum predictive value deviates from the measurement by 2.0 °C during increasing heating load and reducing fan duty processes.
(3) Four typical cases are studied with the proposed DRL control strategy. When the system is operated in a completely new environment with DRL algorithm, the controlled junction may fluctuate initially but the DRL soon recovers to adapt itself and eliminate the fluctuations shortly.
(4) The proposed DRL control strategy can save the fan power by 55.7%, 40.3% and 26.3%, respectively, in comparison with the strategy with 100% fan duty. Yet the fan power consumption by DRL algorithm still appreciably lower than that using the strategy having a fixed 40% fan duty with 16.7% energy saving.

CRediT authorship contribution statement

Wen-Xiao Chu: Conceptualization, Writing - original draft. **Yun-Hsuan Lien:** Conceptualization, Experimentation. **Kuei-Ru Huang:** Experimentation. **Chi-Chuan Wang:** Conceptualization, Supervision, Reviewing and revising.

Declaration of competing interest

The authors declare that they have no known competing financial interests or personal relationships that could have appeared to influence the work reported in this paper.

Acknowledgment

The authors would like to thank for the support from the Ministry of Science and Technology of Taiwan, under contract number 108-2221-E-009-058-MY3 and 108-281-E009-519.

References

Al-damook, A., Alkasmoul, F., 2018. Heat transfer and airflow characteristics enhancement of compact plate-pin fins heat sinks–a review. Propul. Power Res. 7, 138–146.
Al-Damook, A., Kapur, N., Summers, J.L., Thompson, H.M., 2016. Computational design and optimisation of pin fin heat sinks with rectangular perforations. Appl. Therm. Eng. 105, 691–703.
Butterbaugh, M., Kang, S., 1995. Effect of airflow bypass on the performance of heat sinks in electronic cooling. Adv. Electron. Packag. 10.
Chen, H.L., Wang, C.C., 2016. Analytical analysis and experimental verification of trapezoidal fin for assessment of heat sink performance and material saving. Appl. Therm. Eng. 98, 203–212.
Chen, H.L., Wang, C.C., 2017. Analytical analysis and experimental verification of interleaved parallelogram heat sink. Appl. Therm. Eng. 112, 739–749.
Chen, H.L., Wang, C.C., 2018. Analysis and experimental verification of weight saving with trapezoidal base heat sink. Appl. Therm. Eng. 132, 275–282.
Cheng, Z.J., Zhao, Q.C., Wang, F.L., Jiang, Y., Xia, L., Ding, J.L., 2016. Satisfaction based Q-learning for integrated lighting and blind control. Energy Build. 127, 43–55.
Chu, W.X., Tsai, M.K., Jan, S.Y., Huang, H.H., Wang, C.C., 2020. CFD Analysis and experimental verification on a new type of air-cooled heat sink for reducing maximum junction temperature. Int. J. Heat Mass Transfer 148.
Claessens, B.J., Vanhoudt, D., Desmedt, J., Ruelens, F., 2018. Model-free control of thermostatically controlled loads connected to a district heating network. Energy Build. 159, 1–10.
Dalamagkidis, K., Kolokotsa, D., Kalaitzakis, K., Stavrakakis, G.S., 2007. Reinforcement learning for energy conservation and comfort in buildings. Build. Environ. 42, 2686–2698.
Deodhar, A., Bhagwat, H., Singh, U., Sankaranarayanan, D., 2015. Coordinated real-time management of return-air-temperature-controlled cooling units in data centers. ASHRAE Trans. 121, 440.
Fazenda, P., Veeramachaneni, K., Lima, P., O'Reilly, U.M., 2014. Using reinforcement learning to optimize occupant comfort and energy usage in HVAC systems. J. Ambient Intell. Smart Environ. 6, 675–690.

Hossain, M.R., 2006. Optimization of Heat Sinks with Flow Bypass using Entropy Generation Minimization. University of Waterloo.
Hua, H., Qin, Y., Hao, C., Cao, J., 2019. Optimal energy management strategies for energy internet via deep reinforcement learning approach. Appl. Energy 239, 598–609.
Jonsson, H., Moshfegh, B., 2001. Modeling of the thermal and hydraulic performance of plate fin, strip fin, and pin fin heat sinks - influence of flow bypass. Ieee Trans. Compon. Packag. Technol. 24, 142–149.
Kanyakam, S., Bureerat, S., 2011. Multiobjective evolutionary optimization of splayed pin-fin heat sink. Eng. Appl. Comput. Fluid Mech. 5, 553–565.
Kazmi, H., Mehmood, F., Lodeweyckx, S., Driesen, J., 2018. Gigawatt-hour scale savings on a budget of zero: Deep reinforcement learning based optimal control of hot water systems. Energy 144, 159–168.
Khattak, Z., Ali, H.M., 2019. Air cooled heat sink geometries subjected to forced flow: A critical review. Int. J. Heat Mass Transfer 130, 141–161.
Klitzke, N.A., Polzer, S.C., Wilkins, W.L., Gilbert, B.K., Haider, C.R., Ieee, 2018. Comparison of junction temperature prediction methods through analysis of isolated 1-d thermal resistance model variables of an application utilizing forced convection of heat sinks. In: Proceedings 2018 34th Annual Semiconductor Thermal Measurement, Modelling & Management Symposium. Ieee, New York, pp. 119–126.
Kuznetsova, E., Li, Y.F., Ruiz, C., Zio, E., Ault, G., Bell, K., 2013. Reinforcement learning for microgrid energy management. Energy 59, 133–146.
Lee, S., 1995. Optimum design and selection of heat sinks. Ieee Trans. Compon. Packag. Manuf. Technol. A 18, 812–817.
Li, H.Y., Chen, C.L., Chao, S.M., Liang, G.F., 2013. Enhancing heat transfer in a plate-fin heat sink using delta winglet vortex generators. Int. J. Heat Mass Transfer 67, 666–677.
Li, H.Y., Chiang, M.H., Lee, C.I., Yang, W.J., 2010. Thermal performance of plate-fin vapor chamber heat sinks. Int. Commun. Heat Mass Transfer 37, 731–738.
Li, H.Y., Tsai, G.L., Chao, S.M., Yen, Y.F., 2012. Measurement of thermal and hydraulic performance of a plate-fin heat sink with a shield. Exp. Therm Fluid Sci. 42, 71–78.
Li, H.Y., Tsai, G.L., Chiang, M.H., Lin, J.Y., 2009. Effect of a shield on the hydraulic and thermal performance of a plate-fin heat sink. Int. Commun. Heat Mass Transfer 36, 233–240.
Lin, L., Zhao, J., Lu, G., Wang, X.D., Yan, W.M., 2017. Heat transfer enhancement in microchannel heat sink by wavy channel with changing wavelength/amplitude. Int. J. Therm. Sci. 118, 423–434.
Lucchese, R., Johansson, A., 2019. On energy efficient flow provisioning in air-cooled data servers. Control Eng. Pract. 89, 103–112.
Ma, Y.D., Borrelli, F., Hencey, B., Coffey, B., Bengea, S., Haves, P., 2012. Model predictive control for the operation of building cooling systems. Ieee Trans. Control Syst. Technol. 20, 796–803.
Maji, A., Bhanja, D., Patowari, P.K., 2017. Numerical investigation on heat transfer enhancement of heat sink using perforated pin fins with inline and staggered arrangement. Appl. Therm. Eng. 125, 596–616.
Mnih, V., Kavukcuoglu, K., Silver, D., Rusu, A.A., Veness, J., Bellemare, M.G., Graves, A., Riedmiller, M., Fidjeland, A.K., Ostrovski, G., Petersen, S., Beattie, C., Sadik, A., Antonoglou, I., King, H., Kumaran, D., Wierstra, D., Legg, S., Hassabis, D., 2015. Human-level control through deep reinforcement learning. Nature 518, 529–533.
Ni, J.C., Bai, X.L., 2017. A review of air conditioning energy performance in data centers. Renew. Sustain. Energy Rev. 67, 625–640.
Olivieri, S.J., Henze, G.P., Corbin, C.D., Brandemuehl, M.J., 2014. Evaluation of commercial building demand response potential using optimal short-term curtailment of heating, ventilation, and air-conditioning loads. J. Build. Perform. Simul. 7, 100–118.
Prstic, S., Bar-Cohen, A., 2006. Heat shield—An enhancement device for an unshrouded, forced convection heat sink. J. Electron. Packag. 128, 172–176.
Sara, O.N., Pekdemir, T., Yapici, S., Yilmaz, M., 2001. Heat-transfer enhancement in a channel flow with perforated rectangular blocks. Int. J. Heat Fluid Flow 22, 509–518.
Shaeri, M.R., Yaghoubi, M., 2009. Numerical analysis of turbulent convection heat transfer from an array of perforated fins. Int. J. Heat Fluid Flow 30, 218–228.
Silver, D., Huang, A., Maddison, C.J., Guez, A., Sifre, L., van den Driessche, G., Schrittwieser, J., Antonoglou, I., Panneershelvam, V., Lanctot, M., Dieleman, S., Grewe, D., Nham, J., Kalchbrenner, N., Sutskever, I., Lillicrap, T., Leach, M., Kavukcuoglu, K., Graepel, T., Hassabis, D., 2016. Mastering the game of go with deep neural networks and tree search. Nature 529, 484–+.
Sparrow, E.M., Ramsey, J.W., Altemani, C.A.C., 1980. Experiments on in-line pin fin arrays and performance comparisons with staggered arrays. J. Heat Transfer 102, 44–50.
Valladares, W., Galindo, M., Gutierrez, J., Wu, W.C., Liao, K.K., Liao, J.C., Lu, K.C., Wang, C.C., 2019. Energy optimization associated with thermal comfort and indoor air control via a deep reinforcement learning algorithm. Build. Environ. 155, 105–117.
Watkins, C., Dayan, P., 1992. Q-learning. Mach. Learn. 8, 279–292.
Wei, T.S., Wang, Y.Z., Zhu, Q., 2017. Deep reinforcement learning for building HVAC control. In: Proceedings of the 2017 54th Acm/Edac/IEEE Design Automation Conference.
Xi, L., Chen, J.F., Huang, Y.H., Xu, Y.C., Liu, L., Zhou, Y.M., Li, Y.D., 2018. Smart generation control based on multi-agent reinforcement learning with the idea of the time tunnel. Energy 153, 977–987.
Yang, K.S., Li, S.L., Chen, I.Y., Chien, K.H., Hu, R., Wang, C.C., 2010. An experimental investigation of air cooling thermal module using various enhancements at low Reynolds number region. Int. J. Heat Mass Transfer 53, 5675–5681.
Yu, X.L., Feng, J.M., Feng, Q.K., Wang, Q.W., 2005. Development of a plate-pin fin heat sink and its performance comparisons with a plate fin heat sink. Appl. Therm. Eng. 25, 173–182.
Yuan, T.D., 1996. Computational modelling of flow bypass effects on straight fin heat sink in rectangular duct. In: Twelfth Annual IEEE Semiconductor Thermal Measurement and Management Symposium, Proceedings. pp. 164–168.
Zhang, Z., Chong, A., Pan, Y.Q., Zhang, C.L., Lu, S.L., Lam, K.P., Ashrae, 2018. A deep reinforcement learning approach to using whole building energy model for hvac optimal control. In: 2018 Building Performance Analysis Conference and Simbuild. pp. 675–682.
Zhang, X.S., Li, S.N., He, T.Y., Yang, B., Yu, T., Li, H.F., Jiang, L., Sun, L.M., 2019. Memetic reinforcement learning based maximum power point tracking design for PV systems under partial shading condition. Energy 174, 1079–1090.